Dim Star Fringe Tracking Demonstration On SIM's System Testbed-3

Jens Fischer
Jet Propulsion Lab
4800 Oak Grove Ave
Pasadena, CA 91109
818-393-7625
Jens.Fischer@jpl.nasa.gov

Abstract— The Space Interferometry Mission (SIM) System Testbed-3 has been integrated in JPL's new Optical & Interferometry Development Laboratory. The testbed consists of a three baseline stellar interferometer whose optical layout is functionally similar to SIM's current flight layout. The main testbed objective is to demonstrate nanometer class stability of fringes in the dim star, or science, interferometer while using path length & angle feed-forward control, and while the instrument is integrated atop a flight-like flexible structure. This document addresses completion of the Path Length Feed Forward milestone, which requires at least 40 dB of external delay rejection at some frequency between 0.1 and 1.0 Hz.

TABLE OF CONTENTS

1. INTRODUCTION

The Space Interferometry Mission (SIM) System Testbed-3 (STB3) phase 2 has been integrated at the Jet Propulsion Laboratory (Building 318-101). Figure 1-1 shows the testbed with the collector bays on the near and far ends, and with the combiner bays in the center
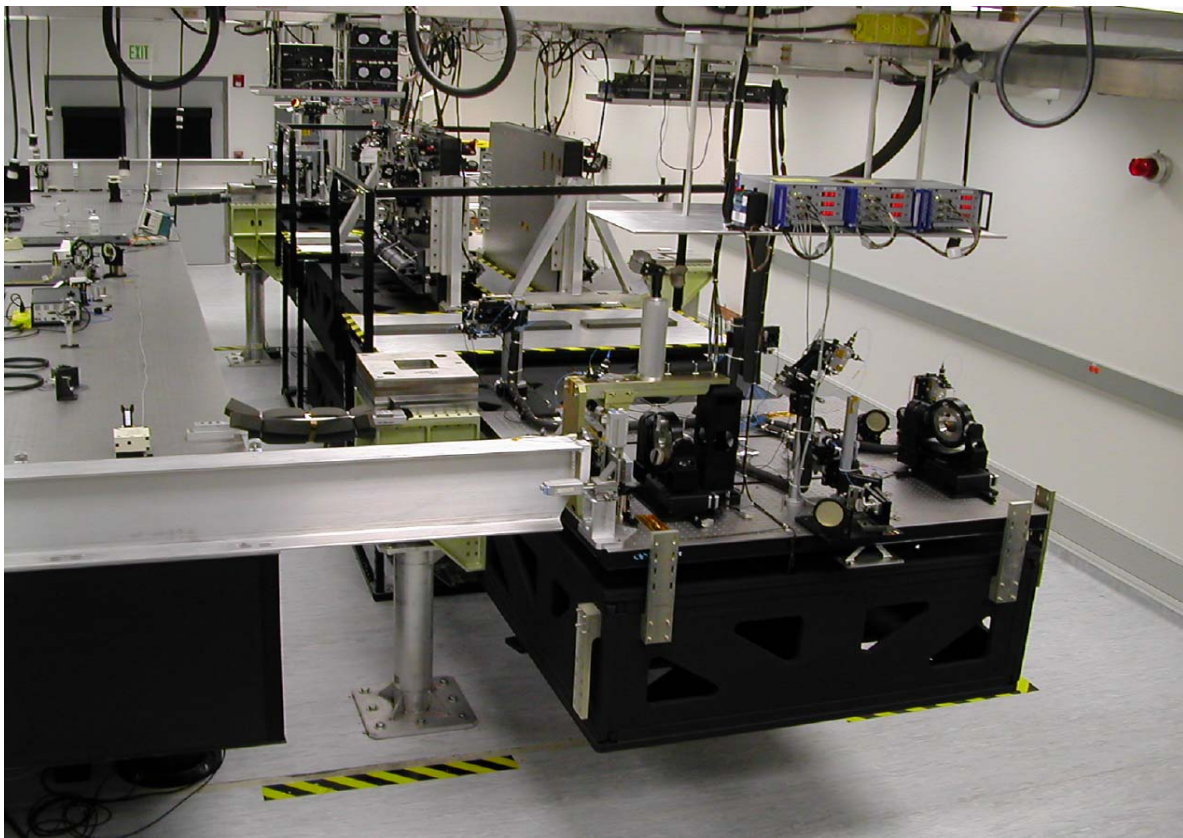

Figure 1-1 STB3 in low bay of Optical & Interferometry development lab

of the picture. The testbed instrument is designed to have the functionality of SIM's Flight System, and is charged with demonstrating nanometer-class fringe stability using the Path Length Feed Forward (PFF) Technique. Goullioud *et al* [1] have already demonstrated the viability of PFF during the first phase of STB3. This early work was conducted on an optical table with a shared 3-baseline stellar interferometer design (4.5 meter baseline length using a green laser source for the pseudo-star system). In its new configuration STB3 will demonstrate PFF while using the non-common baseline design of SIM, and while integrating the instrument on a flight like 9 meters long structure, which will inevitably deform due to vibrations, acoustics, and thermal gradients. In section 2 we describe the path length feed forward technique and develop a brief mathematical description pertinent to STB3. In Section 3 the system architecture is described in detail, while results are discussed in Section 4.

2. DIM STAR FRINGE TRACKING

Like SIM, STB3 uses fringe-tracking information from two stellar *guide* interferometers to stabilize the fringes on the beam combiner of a third interferometer (the *science* interferometer). This scheme, called "path length feed forward" (PFF), requires that the science interferometer fringes be stabilized using the measured fringe tracking delay corrections from the guide stars and an external metrology system measuring the deformations of the precision support structure.
The full form of the PFF algorithm is derived here.

Consider the stellar interferometer shown in Figure 2-1. Assume that a star has already been acquired and
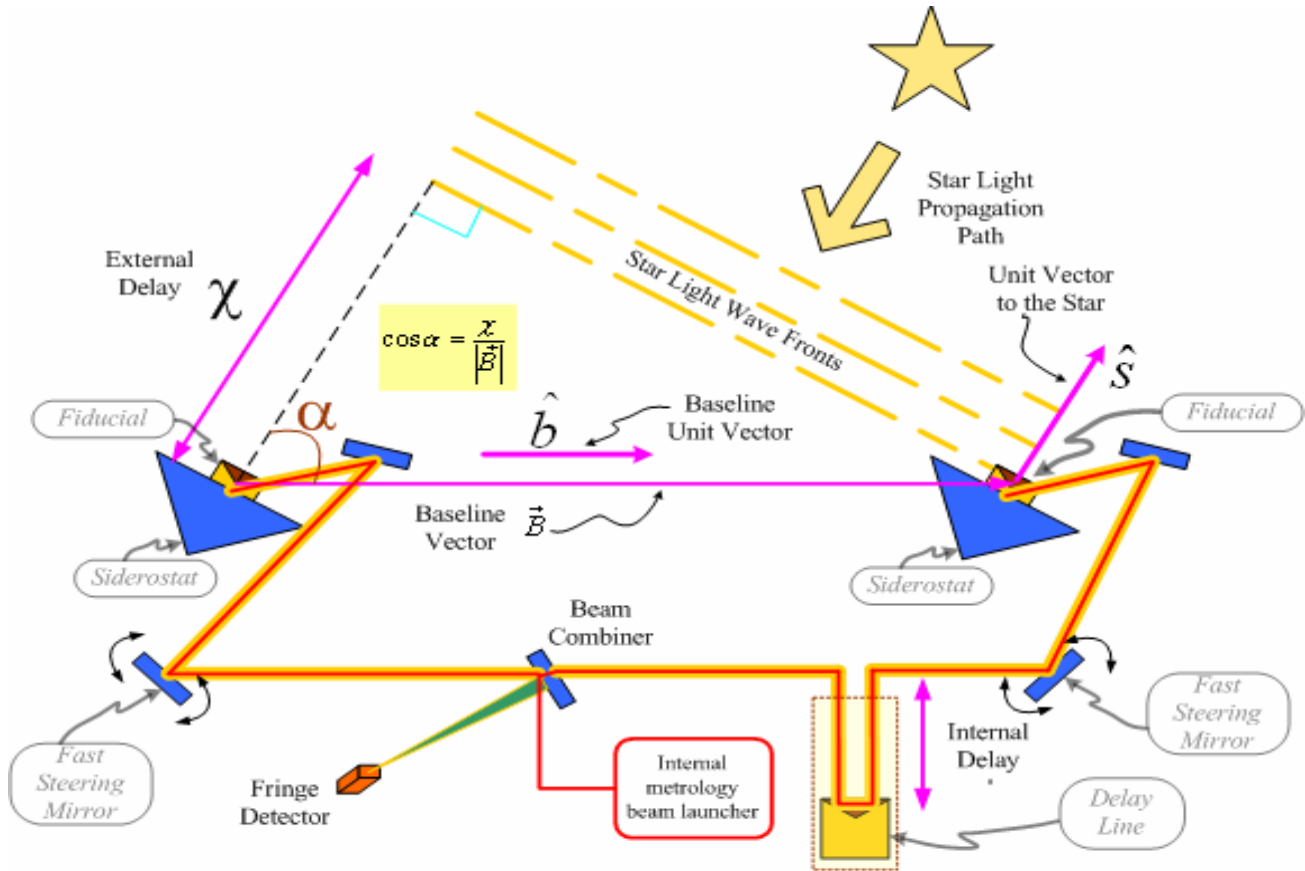

$$\cos\alpha = \frac{\chi}{|\vec{B}|}$$

Figure 2-1 Stellar interferometer diagram (Fringe contrast is at maximum when internal and external delays are precisely equal)

that the instrument is at an equilibrium point (i.e., external delay is balanced by the internal delay, and the star tracker has acquired the star of interest). Figure 1 shows clearly that the external delay, x, can be expressed in terms of the unit vector from the instrument to its target star, $\vec{s}$, and the baseline vector, $\vec{B}$, joining the two telescopes of the interferometer:

$$x = \vec{s} \cdot \vec{B} \qquad (2.1)$$

Linearization of equation 1 about this equilibrium point yields an equation for perturbations about x:

$$\delta x = \delta \vec{s} \cdot \vec{B} + \vec{s} \cdot \delta \vec{B} \qquad (2.2)$$

Equation 2.2 implies that x has already been compensated for during the star acquisition phase, and therefore subsequent perturbations are small and of the order of the attitude stability of the instrument on orbit. Note that perturbations are also due to structural deformations – though these perturbations are only of a second order nature. In SIM total OPD residuals are required to be 10 nanometers RMS or lower, in order for 1 micro-arc-second astrometry to be possible [2,3]

To achieve this level of stability, we use a combination of active and passive methods. The active method is

PFF, which is mainly used to reject rigid body motion (<10 Hz). The passive method is dual stage isolation of the reaction wheels in the spacecraft, which are the largest source of jitter (> 10Hz). STB3 is charged with demonstrating both the passive and the active techniques together. Bronowicki *et al* discuss the passive isolation technique elsewhere [4].

The science interferometer itself cannot be used to compensate for these perturbations, as its star targets are often too dim and generate photon rates that are too low for sufficient sensory bandwidth. For this reason, the guide interferometers are used to pinpoint the attitude of the instrument with relation to target stars of interest. Fringe tracking information from the guide interferometers is transformed into attitude information for the science interferometer, which in turn uses the information to compensate for its own perturbations. The only caveat with this approach is the relative motion of the science interferometer baseline vector relative to the guide interferometer baseline vector, which is shared by the two guide interferometers (i.e., non-rigid body deformations of the precision support structure). This motion, due to jitter and thermal distortions, is tracked by the external metrology system, and used together with the information from the guide interferometers to synthesize δx for the science interferometer.

The second term in Equation 2.2 can then be re-written in terms of the external metrology and the guide interferometers tracking information, while the first term is set to zero (the unit vector to the star remains fixed during observations).

$$\delta x_s = \vec{s} \cdot \delta \vec{B}_s = \left(B_s + \delta B_s\right)\left(\delta \vec{b}_s \cdot \vec{s}\right) + \delta B_s \left(\vec{b}_s \cdot \vec{s}\right) \qquad (2.3)$$

Where

$$\delta \vec{B}_s = \left(B_s + \delta B_s\right)\delta \vec{b}_s$$

$\left(B_s + \delta B_s\right) :=$ Science baseline length. Measurement provided by the external metrology system

$\delta \vec{b}_s :=$ Science Baseline unit vector change in orientation. Synthesized from guide interferometer fringe tracking data and external metrology data.

$\delta B_s :=$ Science baseline length change. Also provided by the external metrology system.

Equation 2.3 represents the path length feed forward corrections used to stabilize the fringes on the science interferometer. The term $\delta\vec{b}_s$ is of interest, as it has to be "solved" for each time δx_s is calculated. To solve for $\delta\vec{b}_s$ we postulate that it can be expressed as a linear combination of the guide star unit vectors:

$$\delta\vec{b}_s = \alpha\hat{g}_1 + \beta\hat{g}_2 + \gamma\hat{g}_1 \times \hat{g}_2 \tag{2.4}$$

where the coefficients α, β, and γ are calculated using internal and external metrology data and the following system of equations:

$$\delta x_{g_1} = \hat{g}_1 \square \delta\vec{B}_g = \left(B_g + \delta B_g\right)\left(\delta\hat{b}_g \square \hat{g}_1\right) + \delta B_g\left(\hat{b}_g \square \hat{g}_1\right)$$

$$\delta x_{g_2} = \hat{g}_2 \square \delta\vec{B}_g = \left(B_g + \delta B_g\right)\left(\delta\hat{b}_g \square \hat{g}_2\right) + \delta B_g\left(\hat{b}_g \square \hat{g}_2\right) \tag{2.5}$$

$$\left(\hat{b}_s + \tfrac{1}{2}\delta\hat{b}_s\right)\square\delta\hat{b}_s = 0$$

Lets define the parallelism vector, $\vec{e}$, as the difference between the guide interferometers baseline unit vector and the science interferometer baseline unit vector:

$$\vec{e} = \hat{b}_1 - \hat{b}_s \tag{2.6}$$

Substitution of Equations 2.5 and 2.6 into Equation 2.4 yields the following solution for the coefficients in Equation 2.4:

$$\begin{bmatrix} \alpha \\ \beta \end{bmatrix} = \frac{1}{1-\left(\hat{g}_1\square\hat{g}_2\right)^2}\begin{bmatrix} 1 & -\left(\hat{g}_1\square\hat{g}_2\right) \\ -\left(\hat{g}_1\square\hat{g}_2\right) & 1 \end{bmatrix}\begin{Bmatrix} E_1 \\ E_2 \end{Bmatrix}$$

$$\gamma = -\left(\hat{b}_s\square\left[\hat{g}_1\times\hat{g}_2\right]\right) - \sqrt{\left(\hat{b}_s\square\left[\hat{g}_1\times\hat{g}_2\right]\right)^2 - 2\left(\hat{b}_s\square\left[\alpha\hat{g}_1+\beta\hat{g}_2\right]\right)-\left(\left(\alpha\hat{g}_1+\beta\hat{g}_2\right)\square\left(\alpha\hat{g}_1+\beta\hat{g}_2\right)\right)} \tag{2.7}$$

Where E_1 and E_2 are defined below:

$$E_1 = \frac{\delta\chi_{g_1}}{B_g+\delta B_g} - \hat{g}_1\square\delta\vec{e} - \frac{\delta B_g}{B_g+\delta B_g}\left[\hat{g}_1\square\left(\hat{b}_s+\vec{e}\right)\right]$$

$$E_1 = \frac{\delta\chi_{g_2}}{B_g+\delta B_g} - \hat{g}_2\square\delta\vec{e} - \frac{\delta B_g}{B_g+\delta B_g}\left[\hat{g}_2\square\left(\hat{b}_s+\vec{e}\right)\right] \tag{2.8}$$

note that E_1 and E_2 is where the internal and external metrology data come together.

3. SYSTEM ARCHITECTURE

The testbed consists of the stellar interferometer instrument, a precision support structure, a spacecraft bus simulator, a pseudo free-free suspension system, and a star simulator – called the pseudo star. Figure 1-1 shows all of the above as currently assembled in the Low Bay of JPL's Optical & Interferometry Development Laboratory. Not shown in Figure 1-1 is the real time control subsystem, which is located outside of the instrument's bay.
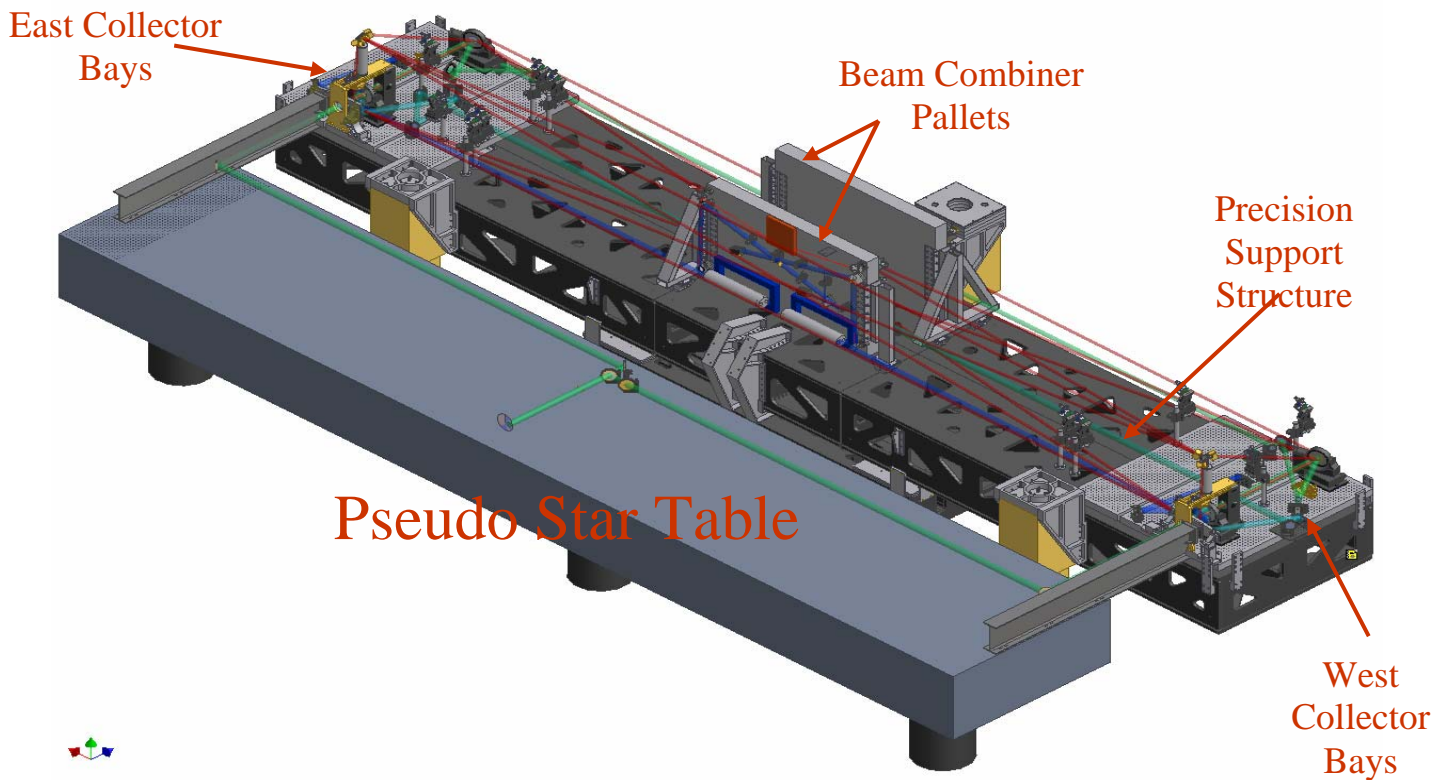
East Collector Bays

Beam Combiner Pallets

Precision Support Structure

Pseudo Star Table

West Collector Bays

Figure 3.1-1 System architecture

3.1 Stellar Interferometer Instrument

The instrument consists of three stellar interferometers (two guide interferometers and one science interferometer) and an external metrology system. Each interferometer consists of two collector bays symmetrically located on each side of a combiner bay. The collector bays for the guide interferometers consist of:

1. A corner cube, or fiducial, which defines the point in space where starlight enters the instrument. This point is also called the "pseudo-pupil" of the guides primary mirrors because it is almost coincident with the transmission grating that generates the stars on each side of the interferometer,
2. A primary mirror located across from the corner cube, which receives the star light in the instrument for the first time,
3. A sequence of reflection mirrors used to relay the star light from the primary mirror to the fast steering mirror, and from the fast steering mirror to the combiner bay

4. A fast steering mirror used in star tracking.

The collector bays for the science interferometer consist of:

1. A corner cube, or fiducial, which defines the point in space where star light enters the instrument,
2. A primary mirror, which receives the starlight in the instrument for the first time. This mirror is mounted on a siderostat, whose axis of rotation is collocated with the vertex of the corner cube.
3. A fast steering mirror used in star tracking.
4. A sequence of reflection mirrors used to relay the starlight from the fast steering mirror to the combiner bay.

The combiner bays for all the interferometers are essentially equal, each bay consist of:

1. An internal metrology beam launcher, which injects a 2 mm beam into the starlight path from the combiner out to each of the corner

cubes on the collectors and back. This metrology system measures the changes in optical path distance between each of the collector corner cubes and the combiner lens on the combiner bay.

2. One delay line for each collector. Only one of the delay lines is active. The other one is passive.
3. A sequence of reflection mirrors to relay the star light from the delay lines to the beam combiner lens
4. A beam combiner lens, which combines the light from each collector onto a single beam,
5. A optical wedge with a 20 or 25 mm through hole, which allows the core of the star light to propagate without interruption, while deflecting the outer annuli onto two different spots on a CCD camera for star tracking
6. An avalanche photo detector to detect fringes
7. A CCD camera for star tracking each of the starlight from each of the collector apertures.

As described above, the guide interferometers share their baseline, which in turn is separated, but parallel to the science interferometer baseline. The degree of parallelism between the guide and science baselines is very important to the performance of the instrument, as is the length of these baselines. These quantities need to be known precisely and reliably to reduce error during dim star fringe tracking and dim star angle tracking. The baseline length of the stellar interferometer is defined as the distance between the corner cube reflectors on its science interferometer collector siderostats, or as the distance between the pair of corner cube reflectors on the "pseudo-pupils" of the guide interferometers primary mirrors. The parallelism of the guide and science baselines is defined by the difference of the unit vectors along the corresponding baselines.

The range of motion of the science interferometer siderostats makes it impossible for the length of its baseline to be measured directly. Hence, a metrology system is used to measure the inevitable changes in baseline parallelism and length. The metrology system is called the external metrology system, and it tracks changes in distances between the corner cubes defining the interferometric baselines, and a third set of corner cube reflectors placed above the plane defined by the guide interferometers baseline and one of the two science interferometers corner cubes. A total of six corner cubes, also known as fiducials, are tracked by the external metrology system, which makes for fourteen different paths. The data collected by the external metrology system is then used to estimate the length changes in the interferometric baselines, and the changes in their parallelism. Figure 3.1-1 shows all the fiducials in the instruments as well as the beams connecting these fiducial. For a discussion on how the data from the metrology system is used to estimate changes in the science baseline length, and the changes in parallelism between the guide and science baselines see [5].
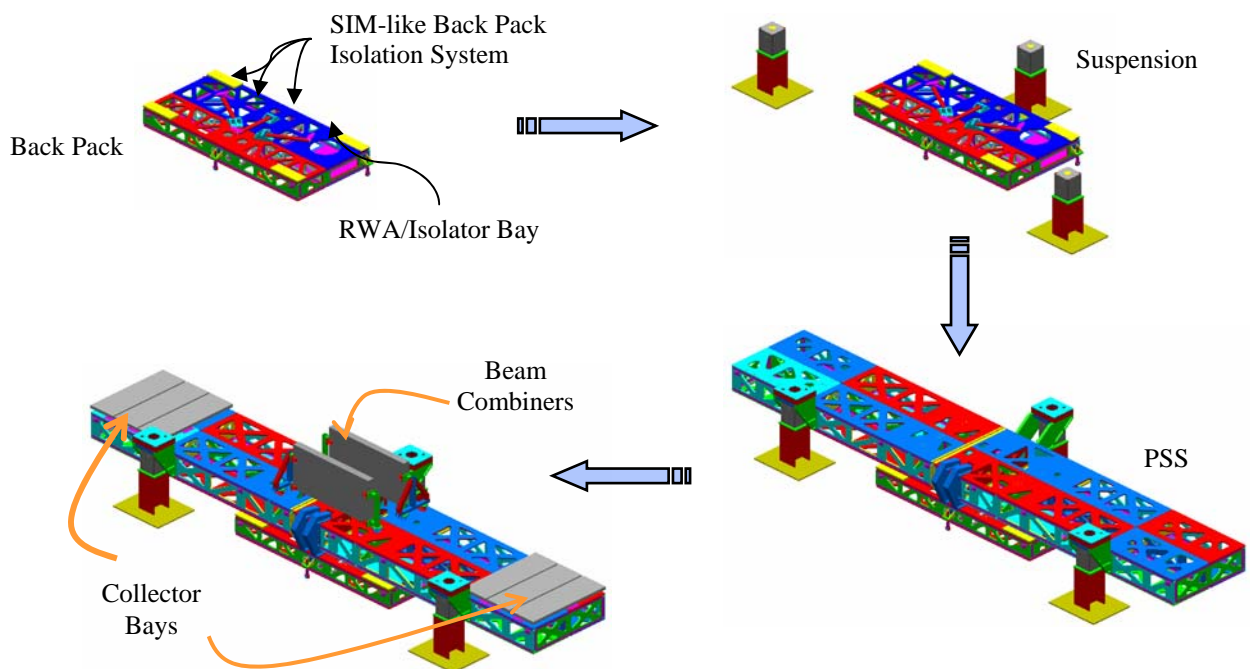

Figure 3.2-1 Assembly of Precision Support Structure, spacecraft simulator (backpack), and suspension system

3.2 Precision support structure, spacecraft bus simulator and pseudo free-free suspension

The precision support structure is where the instrument is mounted; hence, its stability due to jitter, thermal drift, and attitude motion is crucial to the instrument performance as they directly affect fringe contrast and position stability. The required OPD jitter stability for the precision support structure in SIM is 6.6 nm-rms over 1hour above 10 Hz. The precision support structure is a 9-meter long, 1.47-meters wide, and 0.54-meter thick box and panel structure with pseudo kinematic interfaces to the collector and combiner pallets. The structure is constructed with 1 inch thick honeycomb paneling and has shear web panels across

its width at four locations along its length, and a center shear web panel running length-wise along the center of the structure. The spacecraft simulator or backpack is attached to the PSS through a set of 3 bending bars, which provide isolation from the reaction wheels in all 6 degrees of freedom (the reaction wheels are assumed the only source of jitter to the primary support structure. This set up allows for a reaction wheel or some other source of jitter to be placed in the backpack, and test the performance of the isolation system by directly measuring the instrument's performance. Figure 3.2-1 shows how these structures are put together. Note the 3 bending bars on top of the backpack.

A comparison of the dynamics of this structure, with mass simulated instrument, and the dynamics of the current SIM flight system design (with mass simulated instrument as of 3 months ago) showed that the structures are sufficiently similar in response to reaction wheels excitation. Hence, structural modeling techniques developed and validated in STB3 may be used by the SIM flight system. Figure 3.2-2 shows a comparison of STB3's and SIM's response to reaction wheel excitation. The discrepancies between the transfer functions shown have to do with the free-free vs. Pseudo free nature of the systems at low frequencies, and lack of isolator model fidelity in the SIM flight system model at higher frequencies.

3.3 Star simulator

The star simulator, also called the pseudo star system, is an inverse Michelson interferometer generating two identical wave fronts from an optical fiber (east and west arms of the interferometer). The two wave fronts generated are relayed to each of the collector bays on the instrument 8.02 meters apart (beam center to beam
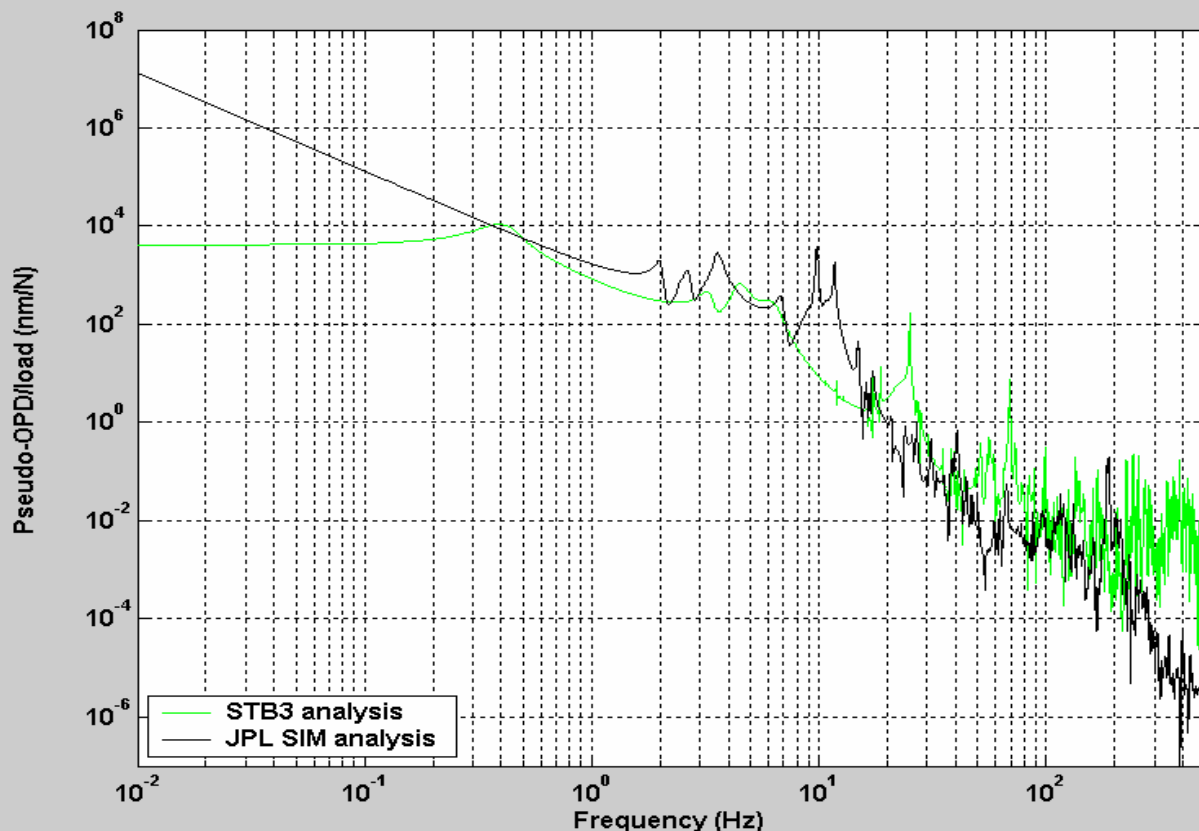

Figure 3.2-2 Comparison of STB3's and SIM's response to on-orbit reaction wheel excitation

center). Three pseudo stars are then generated just before each collector bay (1/4 inch ahead of the guide interferometer's corner cube reflectors) by a diffraction grating system. The refraction gratings create pseudo stars at +/-15.4 degree intervals. The beams of order 0, 1, and –1 are used as the Science, Guide 1 and Guide 2 stars respectively. Figure 3.3-1 shows the output stars from the grating on one side of the instrument. Note that the intensity distribution to the three pseudo stars compared to the source wave is 33% for the science star, 17 % for guide 1, and 4% for guide 2.
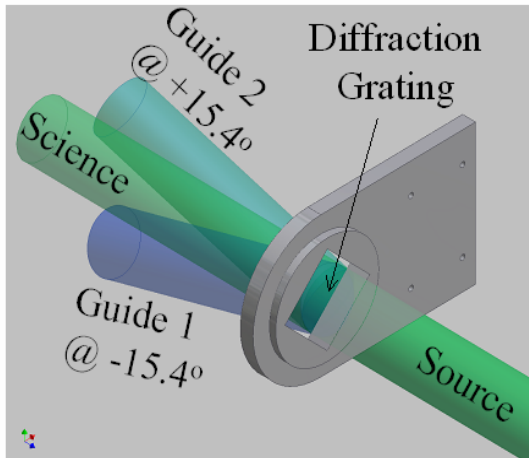
Baseline	% source
Science (0)	33%
Guide 1 (+1)	17%
Guide 2 (-1)	4%

Figure 3.3.1 Star simulator

4. TEST RESULTS

Four sets of results are discussed here: instrument's ambient closed loop internal optical path difference (OPD), instrument's ambient external OPD, the first path length feed forward estimates without external metrology inputs, and path length feed forward measured performance

4.1. Closed loop internal optical path difference

The internal OPD of the instrument's interferometers is measured as the difference in optical path seen by the starlight in one arm of the interferometer versus the other, but measured with the internal metrology system. The internal metrology system is a pencil size

beam injected into the starlight path at the beam combiner pallet, which gets propagated to the corner cubes on the collectors and back to its beam launcher. At the beam launcher, the two returning beams are compared and their phase difference is output as optical path difference (i.e., OPD). In STB3 a large bandwidth control loop based on this measurement is used to stabilize the path seen by the starlight inside the instrument. In other words, the objective of the control loop is to minimize the interferometer's internal OPD. This choice of controls architecture allows the internal metrology beam, a high bandwidth sensor, to sense high bandwidth internal deformations. These deformations would other wise have to be sensed by the fringe tracking control loop. The fringe tracking-only control architecture (i.e., single-loop based on starlight estimates of fringe position) has the disadvantage of requiring the fringe position estimates to have the same bandwidth as the internal jitter bandwidth, which are expected to be lower than the external delay bandwidth of the system (it is unlikely for them to be equal). Such single loop fringe tracking architecture would impose more stringent requirements on the quality of the fringe position estimates. Figure 4.1-1 shows the measured closed loop internal OPD for all three baselines in STB3, along with the corresponding power spectral densities.

Figure 4.1-1 shows 5.14, 4.11, and 1.89 nm-rms for Guide 1, Guide 2 and Science interferometers correspondingly. Note that a large contribution to these OPDs comes from the 25 to 30 Hz portion of the spectrum in all interferometers, which is "*standing*" energy at the isopads in the lab. In addition, the guide interferometers have additional energy in the >100 Hz bandwidth. The motion in the 25 to 30 Hz band comes from lateral motion of the beam combiners, and some of the external metrology beam launcher/mounts. The energy at >100 Hz in the guide interferometers is thought to come from the motion of their corner cube mounts, which are not shared with that of the science interferometer. It is important to note, that these low jitter levels are due largely to the low "G" and acoustic levels in the low bay where the instrument is located. Such environment is slowly being improved as we learn more about the different sources of energy, and take steps to mitigate them.
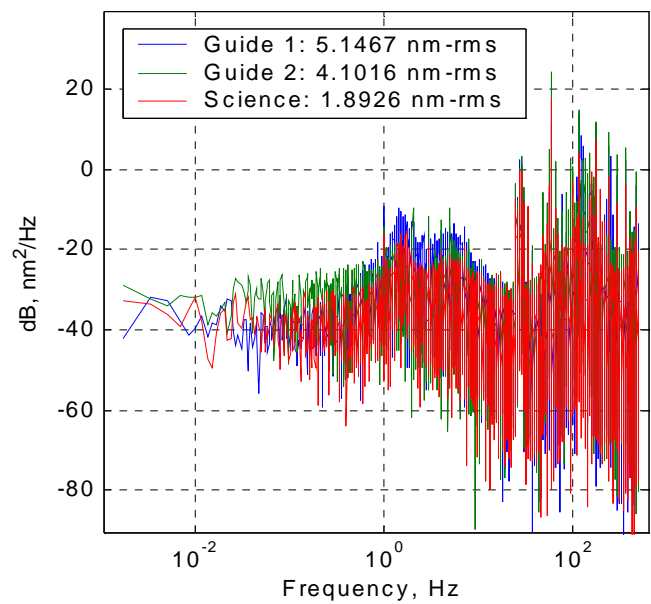
4.2. Instrument's Background-ACS External OPD

The relative attitude motion of the Science interferometer's pseudo star and the science interferometer's baseline can be approximated by a
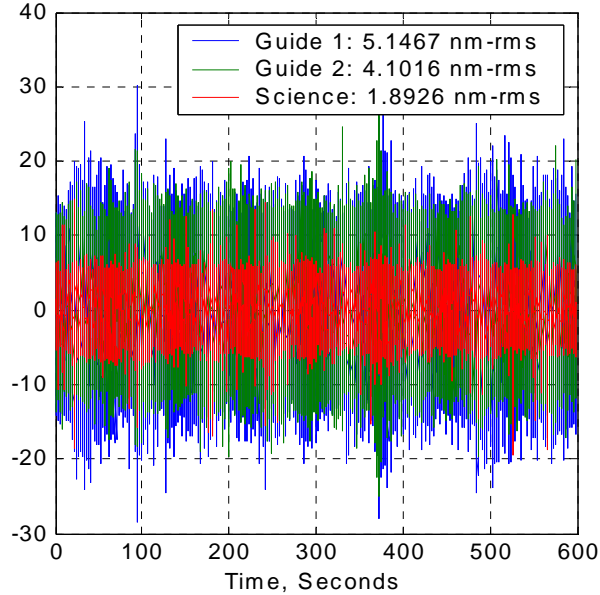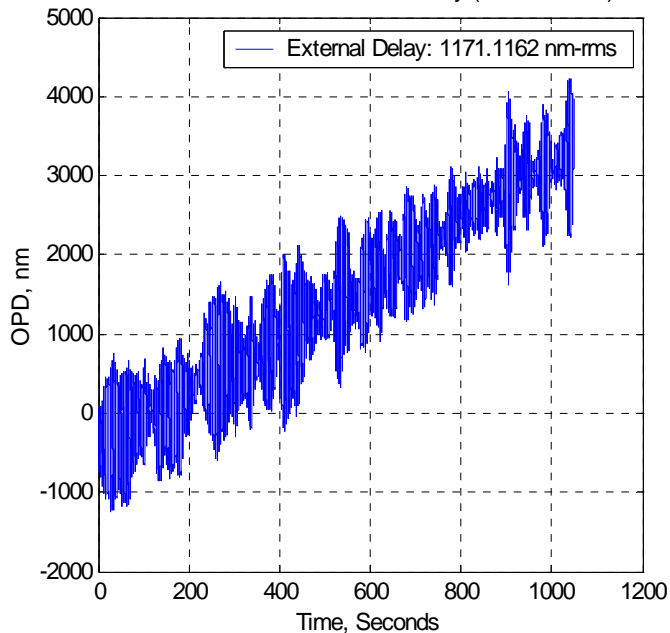
Figure 4.1-1 Measured closed loop internal OPD for all three interferometers in STB3

measurement of the Science interferometer's pseudo star and the guide interferometers' baseline. This measurement is made with a metrology system resident on the Pseudo star table. The output of this metrology system is in nanometers of external delay, which in turn is compensated for by the science fringe tracker. The low frequency portion of the ambient external OPD (DC to 10 Hz) is a result of thermal deformations in the PSS, atmospheric scattering, and relative rigid body motion of the pseudo star table and PSS. The higher frequency portion of the ambient external OPD (>10Hz) is a result of non-symmetric jitter in the PSS.

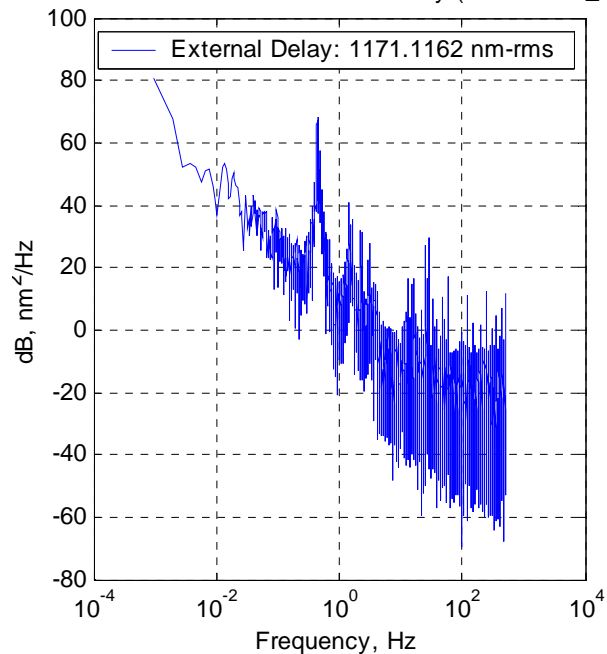Figure 4.2-1 shows about 20 minutes of the science interferometer's external delay as measured by the

pseudo star metrology. This measurement exhibits a typical linear drift (~3000 nm, or 1100 nm-rms, which is the same order of magnitude as the SIM flight system attitude stability requirement), suspension motion (406 nm-rms at 0.5 Hz), backpack isolator motion (6 modes between 1 and 5 Hz, 27.9 nm-rms), and PSS related non-symmetric jitter motion (11 nm-rms from 5 Hz to 500 Hz). This last component should be compared to the SIM flight system required level of external delay at 6.6 nm-rms. Finally, note that of the 11 nm-rms of jitter above 5 Hz, 8.45 nm-rms are concentrated in the frequency band between 25 and 30 Hz.

Figure 4.2-1 Measured background-ACS Science Interferometer External Delay

4.3. Rigid body PFF approximation and simulated performance

The PFF equations were discussed in Section 2, where the external metrology system was shown to be a contributor to the PFF fringe tracking command for the science interferometer. However, this contribution to the PFF command is very small (only a few nanometers are contributed by the external metrology, most of which is likely to be low frequency error due to the atmosphere – as show by early experiments), hence the PFF equations derived in Section 2 were reduced to a simple linear combination of the guide interferometers internal metrology output, with the coefficients being identical. This simplification is possible by assuming a rigid body system, with parallel baselines.

$$\delta\chi_s = \left(\frac{1}{2\cos(15.4^o)}\right)\left[\delta\chi_{g_1} + \delta\chi_{g_2}\right]$$

(4.3-1)

Equation 4.3-1 is accurate to the extent that the system geometry does not change. Using this form of PFF to compute the fringe tracking command for the science delay line and comparing it to the actual science delay line command when all three baselines are fringe-tracking yields a good diagnosing tool. The residual of this comparison yields an idea of where the external metrology might be able to help improve performance, where the performance of fringe tracking in the guide interferometers might be improved, where the system

noise becomes a limitation, and where the atmosphere becomes a limiting factor.

Figure 4.3-1 shows the estimated PFF error. Equation 4.3-1 was implemented using actual fringe tracking data and the result was subtracted from simultaneously recorded Science interferometer fringe tracking commands. This estimate exhibits a linear component (~100 nm or 34.2 nm-rms), which is likely to be the result of thermal expansion, and knowledge error in Equation 4.3-1, a low frequency component (<5 Hz, 17.5 nm-rms) which is likely to be composed of thermal, and atmospheric disturbances, and a jitter component (>5 Hz, 17.5 nm-rms) which is related to PSS jitter and fringe tracking closed loop error at the zero crossing point (note that 15nm-rm of the error above 5 Hz is concentrated at frequencies between 20 and 60 Hz). The data shown in Figure 4.3-1 is encouraging. It is believed that the linear drift plus other thermal related errors in this estimate will be alleviated by the use of the full PFF equations (i.e., external metrology data). Also, error associated with the 20 to 40 Hz regime could be alleviated by a judicious redesign of the fringe tracking loops – though this would required better fringe estimate SNR at frequencies above 20 Hz.

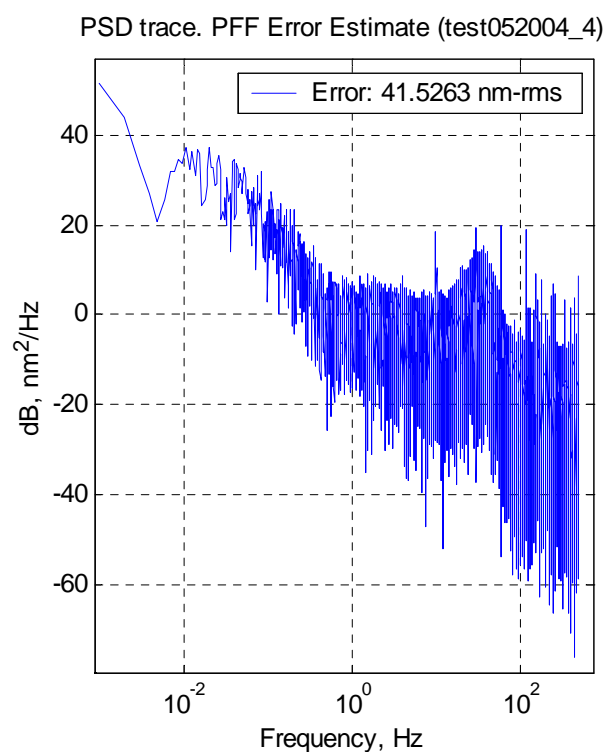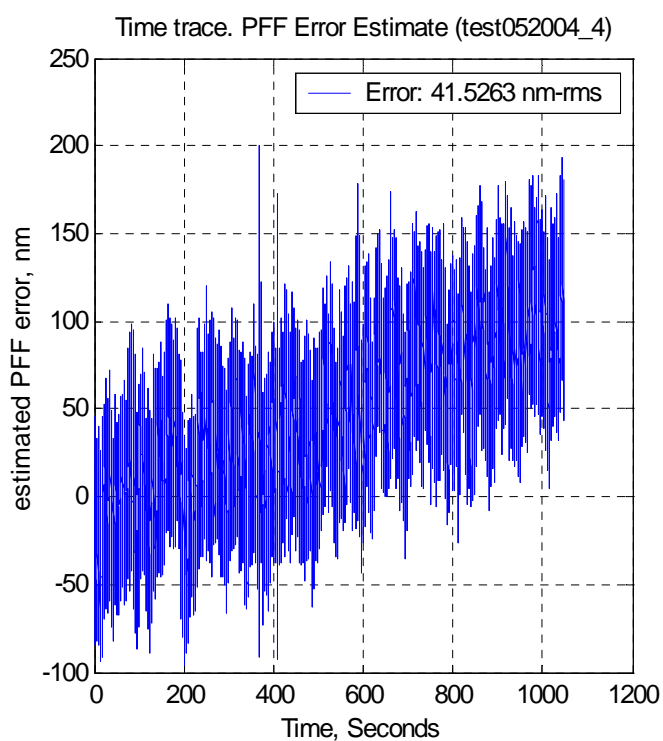## 4.4. Science baseline fringe tracking measurements using Path Length Feed Forward technique

Figure 4.3-1 Estimate of PFF error = difference of PFF (rigid body version) estimated command and Actual PFF command during Science star fringe tracking

This section discusses fringe-tracking performance of the science interferometer in STB3 while on PFF mode. Figure 4.4-1 shows a time plot of the measured external delay seen by the science interferometer (i.e., tracking target), and the optical path difference (OPD) or phase residual measured by the fringe sensor on the science interferometer. Data from the fringe sensor is never used in tracking the fringes. Figure 4.4-1 shows a 20-minute fringe tracking experiment during which the ACS system injected a harmonic ACS disturbance (i.e., external delay) of about 2200 nm-rms at 0.01 Hz (maximum current ACS capability), which divided by the instrument's 8meter baseline results in about 0.06 arc-seconds. Figure 4.4-1 also shows the phase residual for the science interferometer while on PFF mode. The residual shown here was 38.2 nm-rms, which includes both drift and broadband contributions. The total drift in the PFF residual contributes about 26 nm-rms to the total error, and it is largely due to drift in the internal metrology sources (all three interferometers). The atmosphere's contribution to the total low frequency error (i.e., <1 Hz) is estimated to be in the neighborhood of 6 to 10 nm-rms (this estimate is actually based on external metrology data).

Figure 4.4-2 shows the power spectral density for the data shown in Figure 4.4-1. Figure 4.4-2 shows about 50 dB of rejection at about 0.5 Hz for the Science interferometer. Figure 4.4-2 also shows about 60 dB of rejection at 0.01 Hz (the limiting factors in measuring the actual performance at 0.01 Hz are the ACS range and the noise floor). Figure 4.4-2 clearly shows that the PFF performance requirement has been met (i.e., STB3 has demonstrated better than 40 dB of rejection at a frequency in the 0.1 to 1.0 Hz band).

Figure 4.4-3 shows the integrated PSD for the de-trended (linear trend removed) residual phase shown in Figures 4.4-1 and 4.4-2. Figures 4.4-3 shows both the forward and backward integration of the PSD. This figure shows the error below 10 Hz to be about 14 nm-rms, which is better than a factor of 2 improvement over the noise floor attained during STB3's first phase. Also evident from Figure 4.4-3 are the contributions to the error from several frequency bands (25 to 29 Hz, 58 Hz, 115 Hz), which contribute motion to the fringes (total contribution is about 20 nm-rms). This motion is largely outside the fringe tracking control bandwidth (zero crossing is at about 30 Hz for the guide interferometers) and hence cannot be reduced. The modes of jitter at the aforementioned frequency bands are largely understood as deformable modes of the instrument, which are observable by the fringe detector (i.e., the motion results in external delay, even when the internal metrology system is successful at "freezing" the internal path). The source of excitation is laboratory's acoustic background and ground jitter.
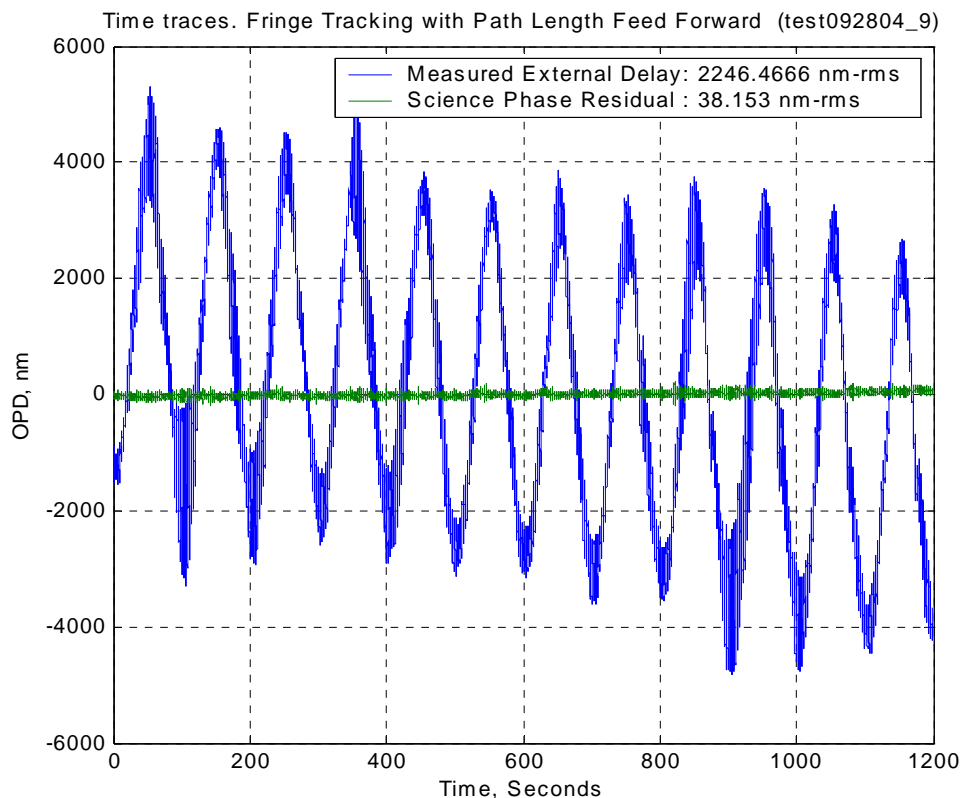

Figure 4.4-1 Path length feed forward performance on Science interferometer: time plot

5. CONCLUSIONS

A short derivation of the path length feed forward algorithm has been presented as well as the new STB3 instrument architecture. Results showing progress towards a sufficiently quiet test environment have been discussed, demonstrating that the testbed is capable of operating at background levels 3X the SIM jitter level stability requirements. PFF error measurements discussed here show that the PFF milestone has been completed without having to use information from the external metrology system.

6. ACKNOWLEDGEMENTS

The results presented are the work of a team. The most recent set of team members is: Arshak Avanesyan, John Shaw, Oscar Alvarez-Salazar, George Sun, Sung Park, Yekta Gursel, Ali Azizi.

7. REFERENCES

[1] R. Goullioud, O.S. Alvarez-Salazar, and B. Nemati, "Path feed forward performance of an astrometric 3-BL interferometer testbed (STB-3)," *SPIE conference on Interferometry in Space*, vol. 4852, 2002

[2] R. A. Laskin, "SIM technology development overview -light at the end of the tunnel," *SPIE conference on Interferometry in Space*, vol. 4852, 2002.

[3] J. Marr, "Space Interferometry Mission (SIM) overview and current status," *SPIE conference on Interferometry in Space*, vol. 4852, 2002.

[4] A. J. Bronowicki, R. MacDonald, Y. Gursel, R. Goullioud, T. Neville, D. Platus, "Dual stage passive vibration isolation for optical interferometer missions," *SPIE conference on Interferometry in Space*, vol. 4852, 2002

[5] Alvarez-Salazar, R., Azizi, A. "Space Interferometry Mission System Testbed-3: External Metrology Inversion," IEEE Aerospace Conference, Big Sky, Montana, March 2004